Deep Silicon Etching for X-Ray Diffraction Devices Fabrication

Houxun Miao[1], Mona Mirzaeimoghri[1, 2], Lei Chen[3], and Han Wen[1]
[1] National Heart, Lung, and Blood Institute, National Institutes of Health, Bethesda, MD 20892, USA
[2] Department of Mechanical Engineering, University of Maryland, College Park, MD 20742, USA
[3] Center for Nanoscale Science and Technology, National Institute of Standards and Technology, Gaithersburg, MD 20899, USA
E-mail: houxun.miao@nih.gov

***Abstract*—We report deep reactive ion etching of silicon gratings via cryogenic and Bosch processes. An aspect ratio of > 50 is achieved for 400 nm period gratings with both processes.**

***Keywords*—cryogenic silicon etching, Bosch process, x-ray gratings**

I. Introduction

X-ray modalities account for the majority of medical imaging procedures worldwide. The partial absorption of x-ray that passing through the object remains the primary contrast mechanism since the invention of x-ray in 1895. The absorption contrast for soft tissues is very low in the hard x-ray regime (20 keV to 100 keV) used in medical imaging. X-ray phase shift introduced by low absorption materials is in principle 3 orders of magnitude higher than the linear attenuation of the amplitude.

We recently developed an x-ray polychromatic far field interferometer [1] using home-fabricated x-ray diffraction gratings of submicron periods. With the phase and decoherence contrasts, we demonstrated a sensitivity improvement of more than an order of magnitude compared to a commercial digital mammographic scanner. Small period gratings promotes high sensitivity and/or compact setup. However, the fabrication of submicron and deep submicron period hard x-ray gratings is still a challenging task, especially for high photon energy x-rays, owing to the fact that the refractive index difference is extremely small between different materials. The small refractive index contrast requires high aspect ratio gratings. For examples, for Au/Si gratings, a π phase shift at 30 keV requires 7.0 μm depth, while for Si/air gratings, the required depth is 38.5 μm.

We fabricated 200 nm and 400 nm periods x-ray gratings by deep reactive etching of Si gratings, coating Pt on the entire grating surface as seed layer with Al_2O_3 in between as adhesion layer, and filling the trenches with Au via conformal electro-deposition [2]. Deep silicon etching is a crucial step in the fabrication process. Beyond x-ray devices, deep Si etching is an important step in many fabrication processes with broad applications in microelectromechanical systems (MEMS), deep trench capacitors, and through-silicon-via packaging, etc. Here we report our work on deep reactive ion etching of silicon gratings using cryogenic and "Bosch" processes. For 200 nm period gratings, an aspect ratio of 44 was achieved using cryogenic process. For 400 nm period gratings, an aspect ratio of > 50 was achieved with both cryogenic and Bosch processes.

II. Sample Preparation

Cr-on-polymer masks were patterned for cryogenic process. Grating patterns of 200 nm or 400 nm periods were transferred from master templates to resist spin coated on silicon wafers via nanoimprint lithography. The master templates were patterned via interference lithography and reactive ion etch of silicon. Cr layers of 10 nm each were deposited via electron beam evaporation at a 30° incident angle to the wafer surface from each side of the grating lines. The residual resist layer was removed via O_2 plasma.

SiO_2 masks were patterned for Bosch process. A layer of 300 nm SiO_2 was grown on a silicon wafer in a wet oxidation furnace and 30 nm Cr was coated via electron beam evaporation. Then resist was spin coated and grating pattern was transferred via nanoimprint lithography. The residual layer of the resist was removed via O_2 plasma. Unprotected Cr was ion milled through. SiO_2 was etched through using a C_4F_8-O_2 recipe and residual Cr mask was cleaned using O_2 plasma.

III. Cryogenic Process

Cryogenic process utilizes a plasma of combined SF_6 and O_2 at low temperature (typically -130 °C to -100 °C) to simultaneously passivate the sidewall and etch the bottom of the silicon [3]. The continuous etching process results in vertical sidewalls without observable roughness.

Two different recipes were created for 200 nm period and 400 nm period grating etching. For 200 nm period gratings, a combination of low inductively coupled plasma (ICP) power and low pressure minimized the undercut underneath the mask and allowed deep silicon etch. With a recipe of 700 W ICP power, 30 W radio-frequency (RF) power, 0.8 Pa pressure, 6.0 x 10^{-7} m^3/s SF_6 and 1.3 x 10^{-7} m^3/s O_2 flow rates, an etching depth of 4.4 μm was achieved in 9 min, corresponding to an aspect ratio of 44. Fig. 1 shows the cross-section scanning electron microscope (SEM) of the etched grating. The small holes in the etching mask were created as the Cr on top of the resist was punched through at the end of the 9 min etch.

For 400 nm period gratings, a combination of slightly higher ICP power and pressure promotes faster and deeper etching. With a recipe of 1000 W ICP power, 10 W RF power, 1.1 Pa pressure, 8.7 x 10^{-7} m^3/s SF_6 and 1.3 x 10^{-7} m^3/s O_2 flow rates, an etching depth of 10.6 µm was achieved in 10 min, corresponding to an aspect ratio of 53. Fig. 2 shows the cross section SEM of the etched grating.

For both 200 nm period and 400 nm period gratings, the achievable aspect ratio was ultimately limited by the undercut underneath the mask material. We investigated the effect of different mask materials on the undercut and concluded that Cr-on-polymer mask provides the best trade-off between etching selectivity and undercut [4].

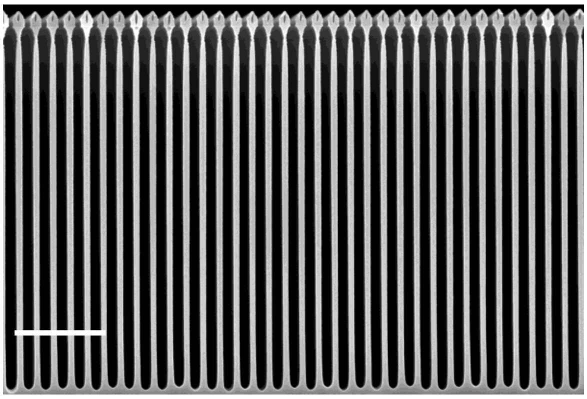

Fig. 1. Cross section SEM image of a 200 nm period grating etched to 4.4 µm via cryogenic process. Scale bar: 1 µm.

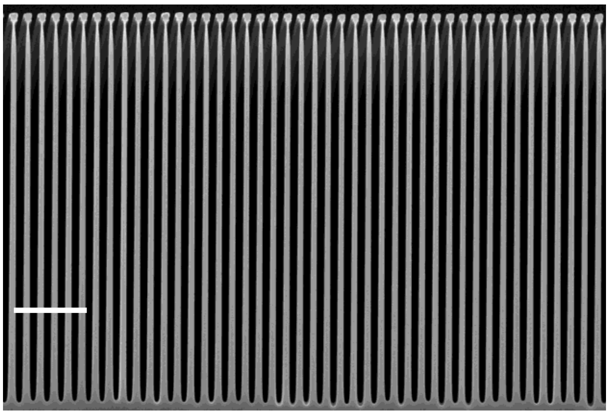

Fig. 2. Cross section SEM image of a 400 nm period grating etched to 10.6 µm via cryogenic process. Scale bar: 2 µm.

IV. Bosch Process

Bosch process alternates SF_6 plasma etching and C_4F_8 plasma passivation steps to obtain directional etching [3]. The switching between etching and deposition steps results in intrinsic scallops. By carefully tuning the etching parameters, the scallops can be reduced. We developed a recipe for 400 nm period grating etching as shown in Table 1. Fig. 3 shows the cross-section SEM image of a grating etched to 11 µm, corresponding to an aspect ratio of 55.

Although, the smoothness and the etching profile are worse than cryogenic process, the undercut underneath the mask is much smaller, which indicates the potential of Bosch process for deeper etching.

TABLE I. Bosch process recipe

Parameters	**Steps**		
	Deposition	***Etch1***	***Etch2***
ICP Power (W)	2500	2500	2500
RF Power (W)	0	50	40
Pressure (Pa)	6.0	3.3	6.7
C_4F_8 (m^3/s)	6.0 x 10^{-6}	0	0
SF_6 (m^3/s)	0	5.0 x 10^{-6}	6.7 x 10^{-6}
Time (s)	1.6	1	1

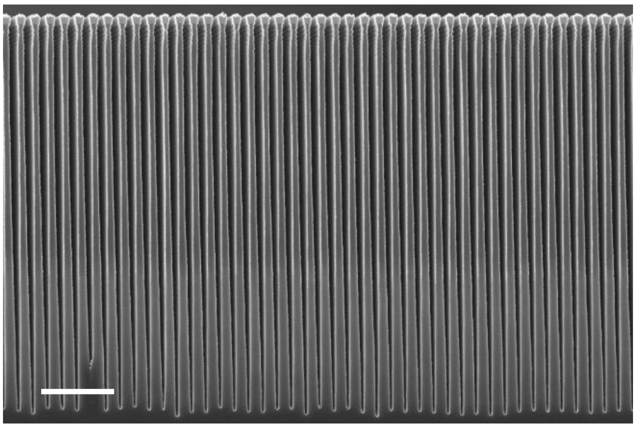

Fig. 3. Cross section SEM image of a 400 nm period grating etched to 11 µm via Bosch process. Scale bar: 2 µm.

V. Conclusion

We demonstrated deep reactive ion etching of submicron silicon gratings via cryogenic and “Bosch” processes. An aspect ratio of 44 was achieved for 200 nm period gratings with cryogenic process. An aspect ratio of > 50 was achieved with both cryogenic and Bosch processes.

Acknowledgment

We acknowledge staffs from the Center for Nanoscale Science and Technology at the National Institute of Standards and Technology for their assistant in fabrication.

References

[1] H. Miao, et al., “A universal moiré effect and application in X-ray phase-contrast imaging,” Nature Phys., vol. 12, pp. 830-834, September 2016.

[2] H. Miao, A. A. Gomella, N. Chedid, L. Chen and H. Wen, “Fabrication of 200 nm period hard x-ray phase gratings,” Nano Lett., vol. 14, pp. 3453-3458, May, 2014.

[3] B. Wu, A. Kumar and S. Pamarthy, “High aspect ratio silicon etch: a review, ” J. Appl. Phys., vol. 108, pp. 051101, September 2010.

[4] H. Miao, L. Chen, M. Mirzaeimoghri, R. Kasica and H. Wen, “Cryogenic etching of high aspect ratio 400-nm pitch silicon gratings, ” J MEMS, vol. 25, pp. 963-967, October 2016.